

Electronic Supplementary Information (ESI)

Inducing Synthesis of Amorphous EuFePt Nanorods and Their Enhanced Effects on Magnetism, Thermostability and Photocatalysis

Ming Wen^{*}, Dan Yang, Qing-sheng Wu^{*}, Ru-ping Lu, Yuan-zheng Zhu and Fan Zhang

Department of Chemistry, Tongji University, Siping Road 1239, Shanghai 200092, China

1. Experiment section

1.1 Chemicals

Dihydrogen hexachloroplatinate ($\text{H}_2\text{PtCl}_6 \cdot 6\text{H}_2\text{O}$, 99%), ferric oxalate ($\text{Fe}_2(\text{C}_2\text{O}_4)_3 \cdot 5\text{H}_2\text{O}$, 99%), europium oxide (Eu_2O_3 , 99%), oleic acid ($\text{C}_{18}\text{H}_{34}\text{O}_2$), sodium hydroxide (NaOH , 99%), Nitric Acid (HNO_3 , 68%), hexane (C_6H_{14} , 99%), ethyl alcohol absolute ($\text{C}_2\text{H}_5\text{OH}$, 99%), propylene glycol ($\text{C}_3\text{H}_8\text{O}_2$, 99%) were all purchased from Sinopharm Chemical Reagent Co., Ltd (SCRC). All the reagents were used without further purification.

1.2 Synthesis of EuFePt nanoparticles

Before the synthesis of FePt and EuFePt alloy nanoparticles, sodium oleate was prepared via 15ml oleic acid reacting with 7g sodium hydroxide under 373K water condition for about 2h, ivory-white product dried in the air. $\text{Eu}(\text{NO}_3)_3$ was prepared via nitric acid with rare earth oxide under water-bath condition for about 2h. Then, $\text{Fe}_2(\text{C}_2\text{O}_4)_3 \cdot 5\text{H}_2\text{O}$, $\text{H}_2\text{PtCl}_6 \cdot 6\text{H}_2\text{O}$ and $\text{Eu}(\text{NO}_3)_3$ were used as precursors to prepare the FePt:Eu nanoparticles. The initial molar ratios of metal ions are 0:56:44 (S0), 1:56:44 (S1), 2:56:44 (S2), 3:56:44 (S3), 5:56:44 (S4), 5:56:44 (S5), 7:56:44 (S6) and 9:56:44 (S7), the component content of obtained EuFePt nanoalloys are $\text{Fe}_{48}\text{Pt}_{52}$, $\text{Eu}_2\text{Fe}_{43}\text{Pt}_{55}$, $\text{Eu}_3\text{Fe}_{41}\text{Pt}_{56}$, $\text{Eu}_4\text{Fe}_{39}\text{Pt}_{57}$, $\text{Eu}_7\text{Fe}_{52}\text{Pt}_{41}$, $\text{Eu}_8\text{Fe}_{41}\text{Pt}_{51}$ and $\text{Eu}_{10}\text{Fe}_{41}\text{Pt}_{49}$, respectively. As far as S5 was concerned, 2 mL ethyl alcohol is mixed with 3mmol of $\text{H}_2\text{PtCl}_6 \cdot 6\text{H}_2\text{O}$, 3mmol $\text{Fe}_2(\text{C}_2\text{O}_4)_3$ and 0.37mmol $\text{Eu}(\text{NO}_3)_3$ at room temperature, then added to sodium oleate (0.2g) . The mixture was dissolved by ultrasonic decomposition. 2 ml oleic acid and 4 ml propylene glycol were injected and the mixture was maintained in the autoclave. The reaction system was sealed and heated at a heating rate of 2 $^\circ\text{C}/\text{min}$ from 20 $^\circ\text{C}$ to 180 $^\circ\text{C}$, and treated at 180 $^\circ\text{C}$ for 15h to 24h. After the reaction was cooled to room temperature, the EuFePt nanorods are collected at the bottom of the container. The as-synthesized products were washed out from the autoclave tube by ethanol with centrifugation thrice, then was re-dispersed and stored in hexane. As contrast, heating rate of 15 $^\circ\text{C}/\text{min}$ was employed to synthesize $\text{Eu}_7\text{Fe}_{52}\text{Pt}_{41}$ nanoparticles with the initial molar ratios of Eu:Fe:Pt=5:56:44 (S4). Detailed data are summarized in Table 1.

1.3 Synthesis of TiO₂

Preparation of TiO₂ nanoparticles was carried out as follows: a parental solution of 5 drops of concentrated HNO₃ and 60ml deionized water was prepared. Then, 10 mL acetic acid was added to 10 mL tetra-*n*-butyl titanate (Ti(OC₄H₉n)₄) and the resulting solution was added drop wise into the above solution under vigorous magnetic stirring. The reaction was carried out in N₂ atmosphere at room temperature for 12h. The semitransparent mixture was sealed in a 100 mL Teflon-lined stainless steel autoclave after filtration, which was filled up to 80% of its total volume, then were calcined in a muffle furnace in air at 160°C for 24 h. TiO₂ nanoparticles can be obtained finally after grinding.

1.4 Characterization

Transmission electron microscope (TEM) images were taken on a JEOL JEM-1200EX microscope (Japan). Scanning transmission electron microscopy (STEM) and elemental maps were carried out under the bright field (BF) mode on JEOL JEM-2100 F microscope. Energy dispersive X-ray (EDX) analysis of nanoalloys was conducted at 20keV on a TN5400 EDS instrument (Oxford). Powder Element analysis of Fe and Pt were measured at $\lambda= 248.3$ nm and 265.9 nm by graphite furnace atomic absorption spectrometer (6810, Shanghai Chromatogram Technology Company, China), and the content of Eu was analyzed through the UV-vis absorbance of Eu complex ($\lambda= 665\text{nm}$) by ultraviolet spectrometer (8453 UV/VIS, Agilent) using arsenazo(III) as chromogenic reagent. X-ray diffraction (XRD) patterns were recorded using Bruker D8 (German) diffractometer with a Cu K α X-ray radiation source ($\lambda= 0.154056$ nm). X-ray Photoelectron Spectroscopy (XPS) experiments were carried out on a RBD upgraded PHI-5000C ESCA system (Perkin Elmer) with Mg K α radiation ($h\nu=1253.6$ eV) or Al K α radiation ($h\nu=1486.6$ eV). In general, the X-ray anode was run at 250W and the high voltage was kept at 14.0 kV with a detection angle at 54°. The pass energy was fixed at 23.5, 46.95 or 93.90 eV to ensure sufficient resolution and sensitivity. The base pressure of the analyzer chamber was about 5×10^{-8} Pa. The sample was directly pressed to a self-supported disk (10×10mm) and mounted on a sample holder then transferred

into the analyzer chamber. The whole spectra (0~1100eV) and the narrow spectra of all the elements with much high resolution were both recorded by using RBD 147 interface (RBD Enterprises, USA) through the AugerScan 3.21 software. Binding energies were calibrated by using the containment carbon (C1s=284.6eV). The data analysis was carried out by using the RBD AugerScan 3.21 software provided by RBD Enterprises or XPSPeak4.1 provided by Raymund W.M. Kwok (The Chinese University of Hongkong, China). The simulation sunlight illumination was carried out by 300W middle-pressure Xenon lamp (MPXL) source (PLS-SXE300/300UV/Trusech, China). Thermal stability were characterized by differential scanning calorimeter (DSC) (STA409PC/4/H/Luxx, NETZSCH). Vibration sample magnetometer (VSM) was used to examine the magnetic properties of FePt nanoparticles on lakeshore7312.

1.5 Photocatalytic property test

The photocatalytic activities of the prepared catalysts were evaluated by the degradation of methyl orange solution. The photocatalytic experiment was performed in a reactor. A 300W of MPXL with wavelength from 320 nm to 780nm was used as an up to down perpendicularity simulation sunlight source. After the as-synthesized EuFePt nanoalloys were treated under decompression drying in vacuum desiccators for 2h at room temperature, 30mg of TiO₂ nanoparticles catalyst simply mixed with 1mg dried FePtEu nanoalloys were added into 40ml of methyl orange solution (50mg/L), and the resulting solution was dispersed by supersonic wave for 15mins. The suspension solution was poured into the photocatalytic reactor, 30 minutes for adsorption and desorption equilibrium before irradiation. During the reaction, 5ml of suspensions mixed solution was withdraw periodically from the reactor chamber, followed by centrifugation and filtration, the obtained clear solution was analyzed by ultraviolet spectroscopy (8453 UV/VIS, Agilent). The degradation rate of methyl orange was calculated by the following equation: D=((C₀-C)/C₀)×100% , where C₀ stands for the initial concentration of methyl orange solution; C stands for the concentration of methyl orange solution after MPXL irradiation at any time.

2. Element analysis and magnetic data of as-prepared nanoalloys

Table S1. Molar ratios of metal ions in initial solution and as-obtained EuFePt nanoalloy composition with their saturation magnetization (M_s) and coercivity (H_c) of as-synthesized (a) and annealed ones (b).

Sample No.	initial molar ratios of EuFePt	Alloy content (at.%)	M_s (emu/g)		H_c (Oe)	
			a	b	a	b
S0 (nanoparticles)	0:54:45	Fe ₄₈ Pt ₅₂	0.42	0.58	710	1262
S1 (nanospheres)	1:54:45	Eu ₂ Fe ₄₃ Pt ₅₅	0.39	0.40	753	2167
S2 (nanospheres)	2:54:45	Eu ₃ Fe ₄₁ Pt ₅₆	0.44	0.38	1772	2601
S3 (nanospheres)	3:54:45	Eu ₄ Fe ₃₉ Pt ₅₇	0.39	0.39	742	1643
S4 (nanospheres)	5:54:45	Eu ₇ Fe ₅₂ Pt ₄₁	0.28	0.43	744	1127
S5 (nanorods)	5:54:45	Eu₇Fe₅₂Pt₄₁	0.30	0.64	747	1874
S6 (nanorods)	7:54:45	Eu₈Fe₄₁Pt₅₁	0.40	0.47	740	1680

3. The morphologies and EDX spectra of as-synthesized EuFePt nanoalloys

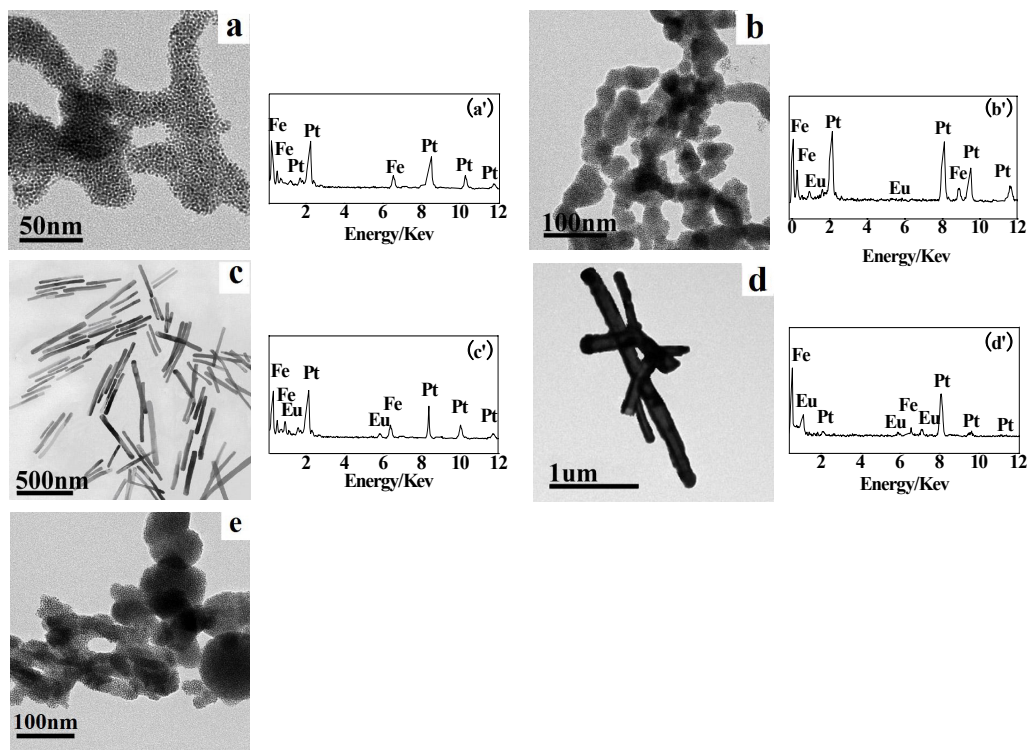


Figure S1. TEM images and EDX spectra of EuFePt nanoalloys obtained at stopping temperature of 180 \square holding for 15h with heating rates of 2 \square /min: a) Eu₃Fe₄₁Pt₅₆ nanoparticles; a') EDS of Eu₃Fe₄₁Pt₅₆; b) Eu₄Fe₃₉Pt₅₇ nanoparticles; b') EDS of Eu₄Fe₃₉Pt₅₇; c) Eu₇Fe₅₂Pt₄₁ nanorods; c') EDS of Eu₇Fe₅₂Pt₄₁; d)

$\text{Eu}_8\text{Fe}_{41}\text{Pt}_{51}$ nanorods; d') EDS of $\text{Eu}_8\text{Fe}_{41}\text{Pt}_{51}$; e) $\text{Eu}_7\text{Fe}_{52}\text{Pt}_{41}$ nanoparticles prepared at the heating rates of $15^\circ/\text{min}$.

4. XRD patterns of as-synthesized EuFePt nanoalloys and annealed at 823K for 5 hours

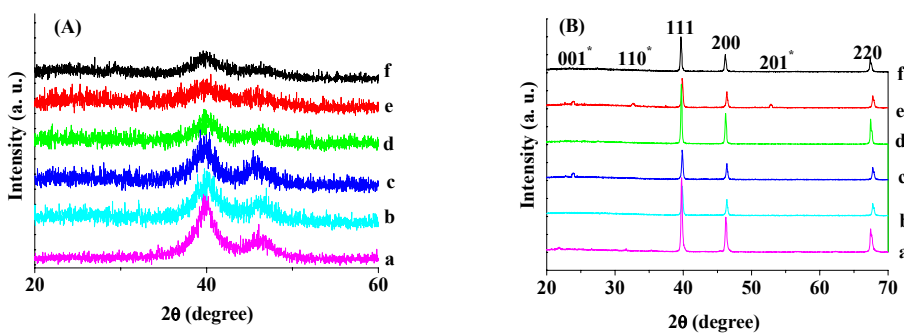


Figure S2. XRD patterns of (A) as-synthesized and (B) annealed specimens:
a) $\text{Fe}_{48}\text{Pt}_{52}$; b) $\text{Eu}_2\text{Fe}_{43}\text{Pt}_{55}$; c) $\text{Eu}_3\text{Fe}_{41}\text{Pt}_{56}$; d) $\text{Eu}_4\text{Fe}_{39}\text{Pt}_{57}$; e) $\text{Eu}_7\text{Fe}_{52}\text{Pt}_{41}$; f) $\text{Eu}_8\text{Fe}_{41}\text{Pt}_{51}$

After the as-prepared EuFePt nanoalloys were annealed at 873K under argon for 5h, the phase transfer to long-range chemically ordered face-center tetragonal (fct) structure ($L1_0$ phase) proved by XRD in Figure S2B. It can be observed that the annealing induced the Eu, Fe and Pt atoms to rearrange into fct structure, as indicated by the (111) and (200) peaks shift and evolution of the (001), (110), (201), (220) peaks, which all peaks corresponding to the formation of superlattice $L1_0$ phase of fct structure. The phase structure of EuFePt nanoalloys are similar to that of the FePt nanoparticles, they all have the diffraction peak of (111), (200), (001), (110), (201) and (220) crystal face corresponding to the fct structure, in which the (201) peak only can be observed in $\text{Eu}_3\text{Fe}_{41}\text{Pt}_{56}$ and $\text{Eu}_7\text{Fe}_{52}\text{Pt}_{41}$, corresponding to the largest coercivity (H_c) of $\text{Eu}_3\text{Fe}_{41}\text{Pt}_{56}$.

5. Room temperature magnetic hysteresis loops of EuFePt nanoalloys for as-prepared and annealed at 823K for 5h.

Lanthanide element of Eu can form intermetallic compound with other metals, the compound of Eu and nonzero magnetic moment 3d metals (Mn, Fe, Co, Ni) is the important magnetic materials. The Eu added EuFePt is expected to have special magnetic property in present work. In order to understand the relation between the compositional dependence of morphology and magnetic property, it is necessary to clear the factors contributing to the present nanoalloy structure. The series of different content of Eu including EuFePt nanoalloys were employed to study the magnetic properties. Figure S3 plots the magnetic hysteresis loops for both as-synthesized and annealed EuFePt nanoalloys. The hysteresis loops were surveyed at room temperature on Lakeshore 7312 vibration sample magnetometer (VSM) under an applied magnetic field of 5000G, in which Sna is the hysteresis loops of as-synthesized nanoalloys and Snb is that of annealed ones. The data of coercivity (H_c) are summarized in Table S1. The H_c of as-synthesized $\text{Fe}_{52}\text{Pt}_{48}$ (S0a), $\text{Eu}_2\text{Fe}_{43}\text{Pt}_{55}$ (S1a), $\text{Eu}_3\text{Fe}_{41}\text{Pt}_{56}$ (S2a), $\text{Eu}_4\text{Fe}_{39}\text{Pt}_{57}$ (S3a), $\text{Eu}_7\text{Fe}_{52}\text{Pt}_{41}$ (S4a), $\text{Eu}_7\text{Fe}_{52}\text{Pt}_{41}$ (S5a), $\text{Eu}_8\text{Fe}_{41}\text{Pt}_{51}$ (S6a) are 710Oe, 753Oe, 1772Oe, 742Oe, 747Oe and 740Oe, respectively. After annealed heating treatment at 873K for 5h under argon, H_c changed to 1262Oe for $\text{Fe}_{52}\text{Pt}_{48}$ (S0b), 2167Oe for $\text{Eu}_2\text{Fe}_{43}\text{Pt}_{55}$ (S1b), 2601Oe for $\text{Eu}_3\text{Fe}_{41}\text{Pt}_{56}$ (S2b), 1643Oe for $\text{Eu}_4\text{Fe}_{39}\text{Pt}_{57}$ (S3b), 1127Oe for $\text{Eu}_7\text{Fe}_{52}\text{Pt}_{41}$ (S4b), 1874Oe for $\text{Eu}_7\text{Fe}_{52}\text{Pt}_{41}$ (S5b), and 1680Oe for $\text{Eu}_8\text{Fe}_{41}\text{Pt}_{51}$ (S6b). The variation of H_c has the parabolic type trend, in which H_c of the annealed $\text{Eu}_3\text{Fe}_{41}\text{Pt}_{56}$ nanoalloys has the largest value of all. In addition, H_c of 1874Oe of $\text{Eu}_7\text{Fe}_{52}\text{Pt}_{41}$ nanorods is higher than 1127Oe of its nanoparticles. It is indicating that both the Eu concentration and the nanoalloys shapes are the most important factor to affect the magnetic properties of ternary EuFePt nanoalloys.

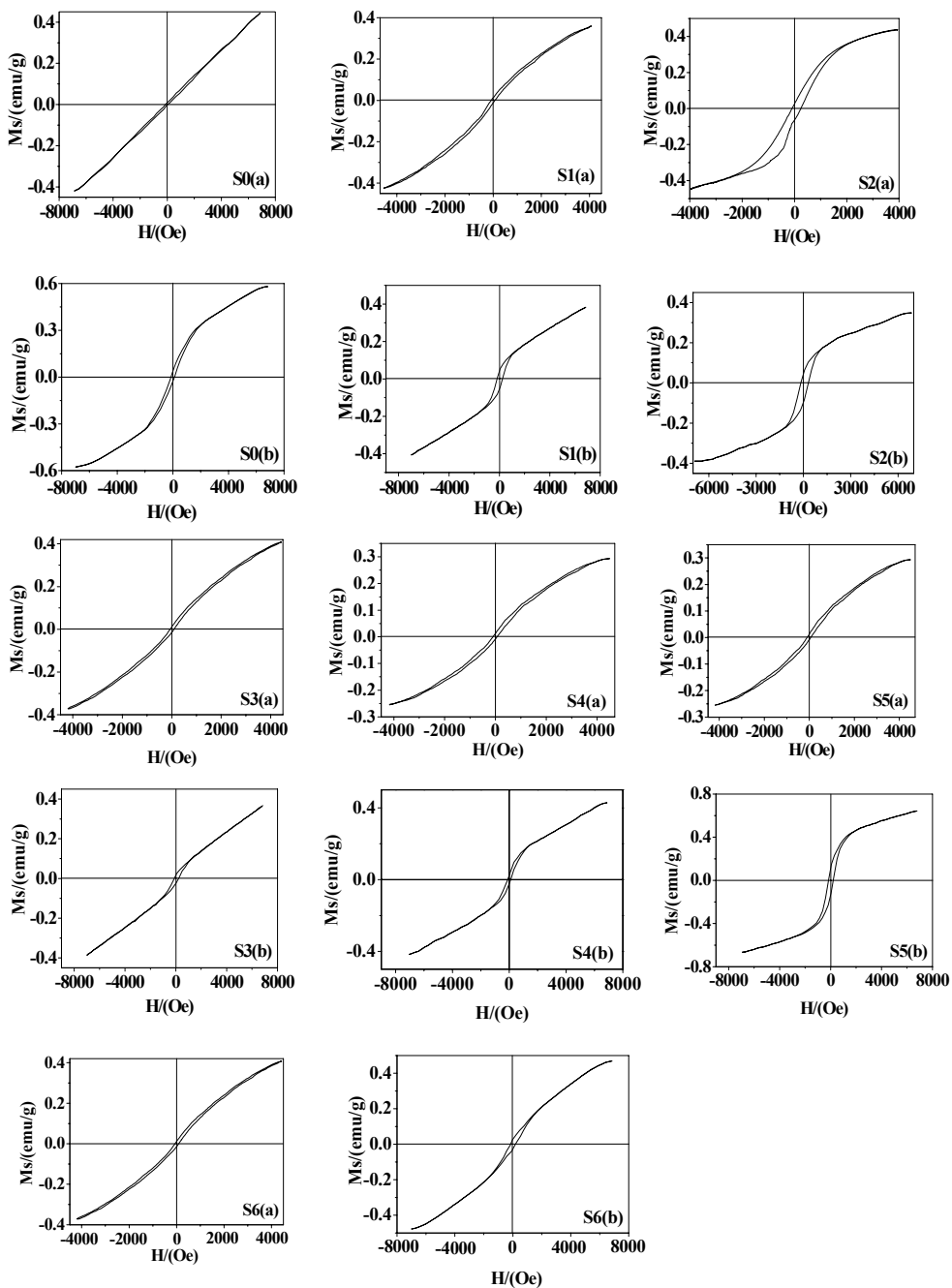


Figure S3. Room-temperature magnetic hysteresis loops of as-prepared (Sna) and annealed ones (Snb): S0) Fe₅₂Pt₄₈ nanoparticles; S1) Eu₂Fe₄₃Pt₅₅ nanoparticles; S2) Eu₃Fe₄₁Pt₅₆ nanoparticles; S3) Eu₄Fe₃₉Pt₅₇ nanoparticles; S4) Eu₇Fe₅₂Pt₄₁ nanoparticles; S5) Eu₇Fe₅₂Pt₄₁ nanorods; S6) Eu₈Fe₄₁Pt₅₁ nanorods.

6. Enhanced effect on photocatalytic activity of TiO_2 by simply mixing with EuFePt nanoalloys.

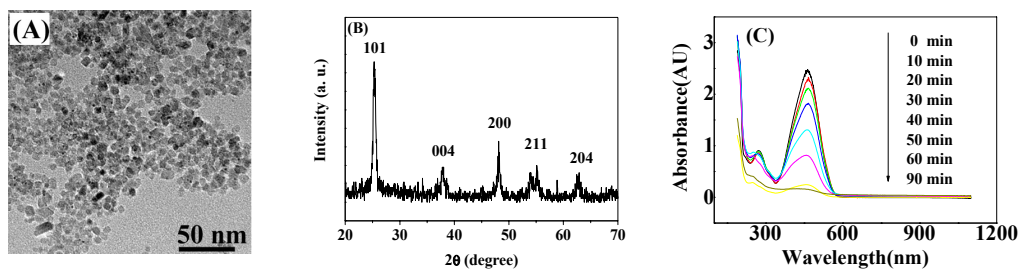


Figure S4. TiO_2 TEM image (A) and its XRD pattern (B) as well as UV-vis absorption spectra for solution separated from TiO_2 nanoparticles suspensions irradiated for various periods (C).

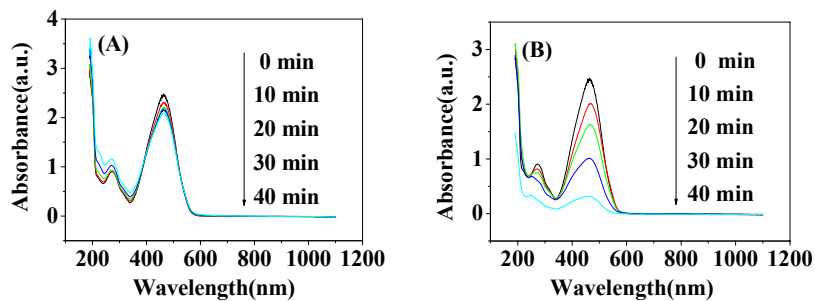


Figure S5. UV-vis absorption spectra for solution separated from (A) Eu₂Fe₄₃Pt₅₅ nanoalloys and (B) TiO_2 + Eu₂Fe₄₃Pt₅₅ mixture nanoparticles suspensions irradiated for various periods.

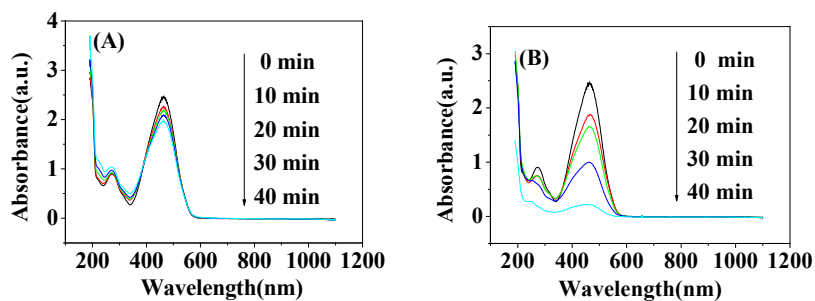


Figure S6. UV-vis absorption spectra for solution separated from (A) Eu₄Fe₃₉Pt₅₇ nanoalloys and (B) TiO_2 + Eu₄Fe₃₉Pt₅₇ mixture nanoparticles suspensions irradiated for various periods.

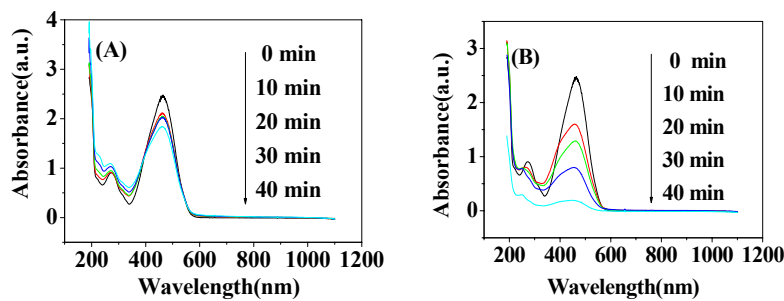


Figure S7. UV-vis absorption spectra for solution separated from (A) Eu₇Fe₅₂Pt₄₁ nanoalloys and (B) TiO₂+ Eu₇Fe₅₂Pt₄₁ mixture nanoparticles suspensions irradiated for various periods.

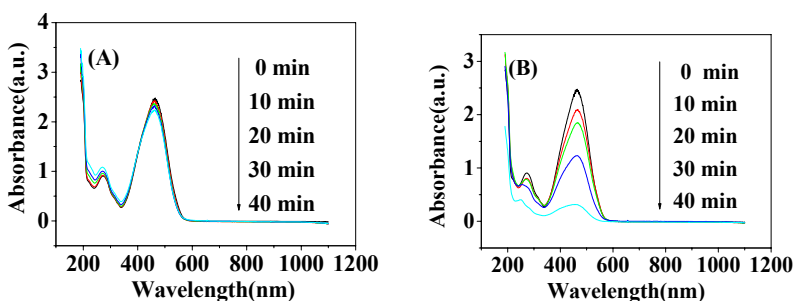


Figure S8. UV-vis absorption spectra for solution separated from (A) Eu₈Fe₄₁Pt₅₁ nanoalloys and (B) TiO₂+ Eu₈Fe₄₁Pt₅₁ mixture nanoparticles suspensions irradiated for various periods.

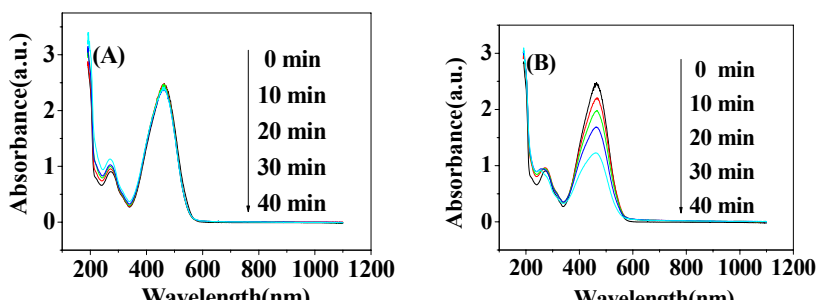


Figure S9. UV-vis absorption spectra for solution separated from (A) Eu₁₀Fe₄₁Pt₄₉ nanoalloys and (B) TiO₂+ Eu₁₀Fe₄₁Pt₄₉ mixture nanoparticles suspensions irradiated for various periods.

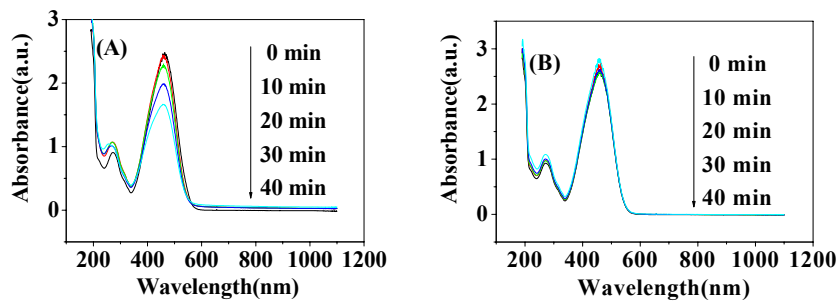


Figure S10. UV-vis absorption spectra for solution separated from (A) Eu_2O_3 nanoparticles and (B) $\text{TiO}_2 + \text{Eu}_2\text{O}_3$ mixture nanoparticles suspensions irradiated for various periods.

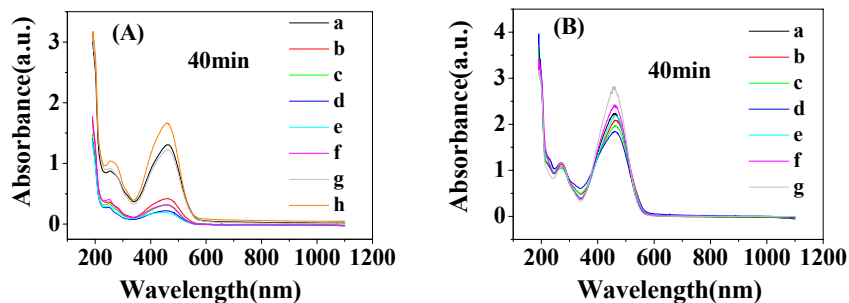


Figure S11. UV-vis absorption spectra for solution separated from photocatalysis nanoparticles suspensions under simulation sunlight irradiated for 40min by a 300W of MPXL source: (A) TiO_2 mixed with FePtEu or Eu_2O_3 nanoparticles: a) TiO_2 ; b) $\text{TiO}_2 + \text{Fe}_{48}\text{Pt}_{52}$; c) $\text{TiO}_2 + \text{Eu}_2\text{Fe}_{43}\text{Pt}_{55}$; d) $\text{TiO}_2 + \text{Eu}_4\text{Fe}_{39}\text{Pt}_{57}$; e) $\text{TiO}_2 + \text{Eu}_7\text{Fe}_{52}\text{Pt}_{41}$; f) $\text{TiO}_2 + \text{Eu}_8\text{Fe}_{41}\text{Pt}_{51}$; g) $\text{TiO}_2 + \text{Eu}_{10}\text{Fe}_{41}\text{Pt}_{49}$; h) $\text{TiO}_2 + \text{Eu}_2\text{O}_3$; (B) EuFePt and Eu_2O_3 nanoparticles: a) $\text{Fe}_{48}\text{Pt}_{52}$; b) $\text{Eu}_2\text{Fe}_{43}\text{Pt}_{55}$; c) $\text{Eu}_4\text{Fe}_{39}\text{Pt}_{57}$; d) $\text{Eu}_7\text{Fe}_{52}\text{Pt}_{41}$; e) $\text{E}_{10}\text{Fe}_{41}\text{Pt}_{51}$; f) $\text{Eu}_{10}\text{Fe}_{41}\text{Pt}_{49}$; g) Eu_2O_3 .